U.S. ARMY COMBAT CAPABILITIES DEVELOPMENT COMMAND
CHEMICAL BIOLOGICAL CENTER
ABERDEEN PROVING GROUND, MD 21010-5424

CCDC CBC-TR-1631

Biologically Derived Magnetite Nanoparticles (mNPs) for Use in Electromagnetic Pulse Shielding

Alena M. Calm
Michael Kim
Joe F. Kragl

RESEARCH AND TECHNOLOGY DIRECTORATE

Alice Savage
Frederick L. Beyer
Scott Walck

U.S. ARMY COMBAT CAPABILITIES DEVELOPMENT COMMAND
ARMY RESEARCH LABORATORY
Aberdeen Proving Ground, MD 21005-5069

Kelley Betts
LEIDOS, INC.
Abingdon, MD 21009-1261

May 2020

Disclaimer

The findings in this report are not to be construed as an official Department of the Army position unless so designated by other authorizing documents.

REPORT DOCUMENTATION PAGE

Form Approved
OMB No. 0704-0188

1. REPORT DATE *(DD-MM-YYYY)*	2. REPORT TYPE	3. DATES COVERED *(From - To)*
XX-05-2020	Final	Apr 2018–Oct 2018

4. TITLE AND SUBTITLE
Biologically Derived Magnetite Nanoparticles (mNPs) for Use in Electromagnetic Pulse Shielding

5a. CONTRACT NUMBER

5b. GRANT NUMBER

5c. PROGRAM ELEMENT NUMBER

6. AUTHOR(S)
Calm, Alena M.; Kim, Michael; Kragl, Joe F. (CCDC CBC); Savage, Alice; Beyer, Frederick L.; Walck, Scott (CCDC ARL); and Betts, Kelley (Leidos)

5d. PROJECT NUMBER

5e. TASK NUMBER

5f. WORK UNIT NUMBER

7. PERFORMING ORGANIZATION NAME(S) AND ADDRESS(ES)
Director, CCDC CBC, ATTN: FCDD-CBR-BM, APG, MD 21010-5424
CCDC ARL; 459 Mulberry Point Rd., 200H, APG, MD 21005-5069
Leidos, Inc.; 3465 Box Hill Corporate Center Dr., Abingdon, MD 21009-1261

8. PERFORMING ORGANIZATION REPORT NUMBER
CCDC CBC-TR-1631

9. SPONSORING / MONITORING AGENCY NAME(S) AND ADDRESS(ES)
CCDC CBC Innovative Development of Employee Advanced Solutions Program

10. SPONSOR/MONITOR'S ACRONYM(S)
CCDC CBC IDEAS

11. SPONSOR/MONITOR'S REPORT NUMBER(S)

12. DISTRIBUTION / AVAILABILITY STATEMENT
Approved for public release: distribution unlimited.

13. SUPPLEMENTARY NOTES
U.S. Army Combat Capabilities Development Command Chemical Biological Center (CCDC CBC) was previously known as U.S. Army Edgewood Chemical Biological Center (ECBC).

14. ABSTRACT:
Modern electronic warfare illustrates the need for innovative yet flexible electromagnetic pulse (EMP) protective capabilities for field-forward electronic equipment and components. The iron ore magnetite is a naturally occurring magnetic rock that can absorb radiation energy. Traditional magnetite nanoparticles (mNPs) produced using physical or chemical means have superparamagnetic properties and are an effective material for radiation shielding. New interest in mNPs from living organisms has arisen after it was discovered that biologically derived mNPs have qualities superior to abiotically produced mNPs, such as high chemical purity, low toxicity, good biocompatibility, and environmentally friendly production. Here, the bacterial mNP producer *Magnetospirillum gryphiswaldense* was used in large-scale microbially derived mNP production, delivering a new material production and functionalization capability to the U.S. Army Edgewood Chemical Biological Center (now the U.S. Army Combat Capabilities Development Command Chemical Biological Center [CCDC CBC]; Aberdeen Proving Ground, MD). These milled and characterized mNPs could eventually be incorporated into an environmentally friendly, soy-based foam to make a customizable and sprayable EMP protective material. In the future, CCDC CBC's investments in synthetic biology, protein engineering, additive manufacturing, and materials science may leverage these mNPs to develop new materials and manufacturing capabilities across the CCDC CBC enterprise.

15. SUBJECT TERMS
Nanoparticle (NP)
Electromagnetic pulse (EMP)
Magnetospirillum gryphiswaldense
Cubo-octahedral
Magnetite nanoparticle (mNP)
Magnetosome

16. SECURITY CLASSIFICATION OF:			17. LIMITATION OF ABSTRACT	18. NUMBER OF PAGES	19a. NAME OF RESPONSIBLE PERSON
a. REPORT	b. ABSTRACT	c. THIS PAGE			Renu B. Rastogi
U	U	U	UU	32	19b. TELEPHONE NUMBER *(include area code)* (410) 436-7545

Blank

PREFACE

The work described in this report was started in April 2018 and completed in October 2018. At the time this work was performed, the U.S. Army Combat Capabilities Development Command Chemical Biological Center (CCDC CBC) was known as the U.S. Army Edgewood Chemical Biological Center (ECBC).

The use of either trade or manufacturers' names in this report does not constitute an official endorsement of any commercial products. This report may not be cited for purposes of advertisement.

This report has been approved for public release.

Acknowledgments

The authors would like to acknowledge and thank the CCDC CBC Innovative Development of Employee Advanced Solutions (IDEAS) Program for funding this project, and Dr. Byeongdu Lee at Argonne National Laboratory (Lemont, IL) for access to his form factor code and for helpful discussions regarding form factor analysis.

Blank

EXECUTIVE SUMMARY

The new era of modern-day electronic warfare illustrates the importance of developing innovative yet flexible electromagnetic pulse (EMP) protective capabilities for field-forward electronic equipment and components. The iron ore magnetite is a naturally occurring magnetic rock mineral with properties that allow it to absorb radiation energy. Magnetite nanoparticles (mNPs), which are known to have superparamagnetic properties, also lend well to a variety of applications including wastewater treatment, magnetic resonance imaging, heavy metal removal, drug delivery, catalysts, terabit-level magnetic storage, and radiation shielding. Although most commercial nanoparticles (NPs) are produced using physical or chemical means, a new interest in the production of NPs derived from living organisms arose when it was discovered that biologically derived NPs have several superior qualities as compared with their abiotically produced cousins. These qualities include high chemical purity, low toxicity, good biocompatibility, and environmentally friendly production.

In this effort, bacterial "foundries" were cultivated and explored for the mass production of uniform microbial mNPs. We hypothesized that the improved crystalline properties of biologically derived mNPs should allow them to outperform traditional, abiotically produced mNPs when used for EMP shielding. By leveraging the in-house, large-scale fermentation capability at the U.S. Army Edgewood Chemical Biological Center (ECBC; now known as the U.S. Army Combat Capabilities Development Command Chemical Biological Center [CCDC CBC]; Aberdeen Proving Ground, MD) along with its microbiological expertise, *Magnetospirillum gryphiswaldense* cultures were established and optimized to bring an entirely new bioproduction capability for mNPs to ECBC. The biologically derived mNPs were characterized and will be developed for future incorporation into an environmentally friendly insulation foam that can be formulated into a customizable spray-on EMP protective material that fits well within the Army's Energy Security and Sustainability Strategy. The large-scale production of biologically derived mNPs will also deliver an entirely new material production and functionalization capability to CCDC CBC. In the future, this new capability could leverage the fields of synthetic biology, protein engineering, additive manufacturing, and materials science in innovative ways toward development of new materials and manufacturing capabilities across the CCDC CBC enterprise.

Blank

CONTENTS

FIGURES

TABLE

BIOLOGICALLY DERIVED MAGNETITE NANOPARTICLES (mNPs) FOR USE IN ELECTROMAGNETIC PULSE SHIELDING

1. INTRODUCTION

The evolution of electromagnetic pulse (EMP) disruptive weapons, such as the Counter-Electronics High-Powered Advanced Missile Project that is currently under development by the U.S. Air Force, has shown that the threat of an EMP attack has moved far from the realm of science fiction and into the real world of modern warfare. It is now conventional wisdom that the threat of EMPs, either natural or man-made, poses considerable risk to critical communications equipment and network infrastructure. Such is the threat that the U.S. military has begun efforts to move critical communications gear into a Cold War-era bunker in the Cheyenne Mountain Complex in Colorado,[1] and has made plans to construct a high-altitude electromagnetic pulse and blast-protected mechanical–electrical building in Fort Greely, AK.[2] This new era in modern-day electronic warfare illustrates the importance of developing innovative yet flexible EMP protection capabilities for critical electronics and communications systems currently utilized in the battlefield. The most common method of protecting electronic equipment against an EMP blast is by placing sensitive equipment within a metal enclosure (called a Faraday cage) that is specifically designed to block electromagnetic fields. However, this solution can be expensive and cumbersome, particularly in field-forward environments.

Engineers working at the University of Nebraska (Lincoln, NE) developed a spray-on conductive concrete capable of shielding against EMP energy. The specialized concrete contains a material called magnetite, which has the ability to absorb microwave energy. When mixed with other carbon and metal components, the magnetite-infused concrete could not only absorb EMPs; it was also able to reflect electromagnetic radiation. The product, which is sprayed onto buildings that require EMP protection, is now being developed commercially. It has been determined to exceed the military's own EMP shielding requirements.[3]

Magnetite nanoparticles (mNPs) can have superparamagnetic properties that lend themselves to a variety of applications, such as catalysts, wastewater treatment, magnetic resonance imaging, heavy metal removal, drug delivery, and even terabit magnetic storage devices. However, the size, quality, shape, and crystallization of these nanoparticles (NPs) greatly affect how they behave, making synthetic approaches that provide for optimal NP size control and crystallization greatly desired.[4] Industrial production of magnetite NPs is generally labor-intensive, expensive, and hazardous to living organisms and the environment. In fact, particles made of magnetite nanospheres are abundant in the airborne particulate pollution that is common in cities. These particles have been found to accumulate in the brain, which makes them an environmental risk for neurodegenerative disorders such as Alzheimer's disease.[5]

Traditionally, most mNPs were produced using physical or chemical means. New interest in the production of mNPs derived from living organisms has arisen since it was discovered that biologically derived mNPs have superior properties, including high chemical purity, low toxicity, and good biocompatibility over their synthetic counterparts.

Magnetotactic bacteria sense and align their motion to the Earth's weak magnetic field[6] using specialized intracellular bacterial organelles termed magnetosomes, which are membrane-bound intracellular structures that contain magnetite nanocrystals. Magnetosomes represent a pioneering new source of mNPs. Not only do they have magnetic properties, but they also offer better biocompatibility, size distribution, and functionalization over synthetically produced magnetite crystals. Ranging from 25 to 130 nm in size, the magnetite crystals within the magnetosomes possess a high degree of crystallographic perfection and permanent magnetization. Moreover, the biologically derived NPs are more environmentally sound to produce, and depending on batch size, they can be scaled to provide exact quantities of material.[7]

Many bacterial species have the ability to reduce and accumulate metal ions within their cells to form metallic and metal oxide NPs through the processes of bioreduction or biosorption.[8] These living metallurgists require much less energy for production than synthetic mNPs and have the added advantage of not depending on hazardous or toxic chemicals for their fabrication. These characteristics make microbial mNPs much more environmentally friendly to produce. Furthermore, the composition, size, and morphology of microbial mNPs are genetically and biochemically determined and are influenced by ambient growth conditions such as oxygenation, incubation time, temperature, or pH. Thus, mNPs can attain organism-specific sizes, shapes (e.g., octahedral, cubic, spherical, or decahedral), and unique features that are not available from more heterogeneous, abiotically produced NPs.[9] Two of these features, a membrane that can be biofunctionalized, as well as the protein chain that connects the mNPs within the cell, cannot be recreated synthetically. These features make microbial mNPs of particular interest in the fields of medicine, biology, and bioremediation for applications such as pathogen detection, drug delivery, magnetic hyperthermia, genetic research, enzyme mobilization, and magnetic resonance imaging (MRI) contrast material. The functionality of a NP is directed by its physical properties, most notably, size, shape, chemical purity, and structural homogeneity.[10]

Because mNPs produced by microbial organisms have been functionally optimized through natural selection over billions of years, it could be reasoned that biologically derived mNPs will outperform traditional abiotically produced mNPs in a variety of militarily relevant applications. This effort aimed to harness the power of natural bacterial "foundries" for the mass production and study of mNPs. Future projects will focus on incorporation into an environmentally friendly, soy-based insulation foam designed to provide a customizable spray-on EMP protection material. The mNPs produced and characterized in this project can be used for a variety of EMP signal-shielding applications that fit well within the Army's Energy Security and Sustainability Strategy.[11] Additionally, mNP production delivers an entirely new NP production and functionalization capability to the U.S. Army Combat Capabilities Development Command Chemical Biological Center (CCDC CBC; Aberdeen Proving Ground, MD), previously known as the U.S. Army Edgewood Chemical Biological Center (ECBC). In the future, CCDC CBC could leverage biologically derived mNPs in innovative ways in synthetic biology, protein engineering, additive manufacturing, and materials science to develop new materials and manufacturing capabilities across the CCDC CBC enterprise.

2. MATERIALS AND METHODS

2.1 Growth of Flask Cultures of *Magnetospirillum gryphiswaldense*

M. gryphiswaldense DSM 6361 strain MSR-1 was obtained from the Leibniz Institute DSMZ-German Collection of Microorganisms and Cell Cultures (DSMZ; Braunschweig, Germany). A live culture was received in a 16 mL Hungate tube and placed in a 30 °C incubator for several days. A modified Hungate technique[12] was used to propagate the strain. Modifications to the technique were made in the following way. The nitrogen gas that was used was not subjected to an oxygen-scavenging copper coil. All cultures were grown in 16 mL Balch tubes (Thermo Fisher Scientific; Waltham, MA) that had been prefilled under nitrogen gas with I culture medium[13] before being sealed and autoclaved for 20 min. All of the culturing techniques and preparation work were performed in a biological safety cabinet (BSC) to provide a clean environment.

Before inoculation, a sterile needle and syringe (Becton Dickenson; Franklin Lakes, NJ) were used to pass 4 mL (5%) of air into the septum and through a 0.2 μm filter (Thermo Fisher Scientific). The seed culture from DSMZ was mixed gently and inverted. One milliliter of inoculum was sterilely transferred into new tubes. Culture tubes were placed in a tube rack at a 45° angle and incubated at 30 °C. Culture growth was monitored every 24 h by measuring the absorbance of light at 600 nm on a Genesys 20 spectrophotometer (Thermo Fisher Scientific). When cultures achieved an optical density (OD) of between 0.05 and 0.1, they were used to inoculate flask cultures. All inoculations were achieved by making a 10% volume-to-volume addition into a new culture; for example, to scale up to a 50 mL culture, a 5 mL inoculum would be introduced into the new flask. All flasks maintained 80% headspace for gas exchange. All flask cultures were incubated at 30 °C and agitated at 100 rotations per minute (rpm). A growth curve was performed by monitoring the OD_{600} and graphing the results. Glycerol stocks were made for future use by mixing a log-phase culture and 50% sterile glycerol (Thermo Fisher Scientific) in a 1:1 ratio. Glycerol stocks were frozen in liquid nitrogen and stored at –80 °C.

2.2 Formation and Verification of Magnetosomes in *M. gryphiswaldense*

After flasks were cultured for 24 h, sterile ferric quinate solution[14] was added to achieve a final concentration of 0.02 mM. Flasks were placed back in the incubator at 30 °C and agitated at 100 rpm overnight. In the morning, a nitrogen overlay was applied for 24 h, and cultures were then collected for analysis. Magnetosome formation was verified by observing the culture color: a shift from white to dark brown was one indicator that magnetosomes had formed. An additional verification method was to observe the attraction of the bacteria to a magnetic field. Ten milliliters of culture was collected, centrifuged, and resuspended in 1 mL of phosphate-buffered saline (PBS; Thermo Fisher Scientific) before it was transferred to a glass 10 mL test tube. The test tube was placed on the benchtop in the horizontal position, and a neodymium iron boron magnet (Thermo Fisher Scientific) was placed at one end. Observations were made after several hours.

2.4 Growth of 20 L Cultures of *M. gryphiswaldense* in a Fermenter

Twenty milliliters of frozen glycerol stock of *M. gryphiswaldense* MSR-1 was used to inoculate 200 mL of culture medium I[13] in a 500 mL flask. The 500 mL flask was incubated at 30 °C and 225 rpm. Log-phase cultures were used to inoculate 1.8 L of medium in a 4 L flask. The 4 L flask was incubated at 30 °C and 175 rpm using an I2500 series incubator shaker (New Brunswick Scientific; Enfield, CT). At log phase, the 2 L cultures were transferred through a presterilized 2 L transfer bottle to inoculate the Micros 30 fermenter, (New Brunswick Scientific) which had been prepared and steam-in-place sterilized with 18 L of culture medium I. The operating parameters for the Micros 30 were 30 °C, 150 rpm, 2 standard liters per minute (slpm), 1 psi overhead pressure, and a working volume of approximately 20 L. The cells at the end of the 20 L fermentation were harvested by continuous centrifugation at 2 L per min. The cell paste was scraped from the centrifuge cores and stored in an –80 ℃ freezer for later processing and purification of the magnetosomes.

2.5 Purification and Storage of mNPs

A frozen aliquot of *M. gryphiswaldense* from a 20 L fermentation was weighed and thawed in a 1:5 weight/volume ratio of PBS buffer, pH 7.2 (Thermo Fisher Scientific), that contained 1× Halt EDTA-free protease inhibitor (Thermo Fisher Scientific). Once thawed, the cell paste was mixed with PBS until the consistency was smooth. The cells were passed through an M110P microfluidizer (Microfluidics; Westwood, MA) at 20,000 psi three times. Magnetosomes were separated from cell debris by using a Dynal magnetic bead separator (Invitrogen; Carlsbad, CA). After separation, the supernatant was aspirated, and the magnetosome content was resuspended in PBS, pH 7.2. This process was repeated 10 times in PBS, pH 7.2. The following storage methods were assessed: drying, storage at 4 °C , and freezing at –80 °C in 25% glycerol. Two different drying techniques were attempted: drying at 60 °C overnight, and drying at room temperature in a BSC on a bed of Drierite absorbent (MilliporeSigma; Burlington, MA) overnight. The total yield of magnetosomes was derived from the dry weight. In both cases, an attempt was made to resuspend the dried magnetosomes in both water and PBS, analysis was carried out via transmission electron microscopy (TEM).

2.6 Characterization and Analysis of mNPs

2.6.1 TEM

TEM was used to evaluate the different storage conditions of the magnetosomes as well as to measure particle size. Magnetosomes were evaluated from several different conditions and solutions. Magnetosomes that had been stored at –80 °C in 25% glycerol were thawed and washed several times in PBS, then resuspended in water or PBS for evaluation. Magnetosomes that were dehydrated were suspended in PBS and water. Magnetosomes that were stored at 4 °C were evaluated in PBS, water, and ethanol. The ethanol samples were first washed in water and then slowly introduced to ethanol by washing and resuspending in a series of increasing concentrations (50, 75, 95, and 100%) with a 10 min incubation between steps. TEM was also used to view magnetosome formation inside of whole bacteria. The whole bacteria were prepared by first fixing them in 10% formalin and then dehydrating them in

ethanol as previously described. Grids for TEM were prepared by drop-casting 5 µL solutions of magnetosomes or bacteria directly onto a 300 mesh Lacey carbon-coated copper grid (Ted Pella; Redding, CA). Magnetosomes and bacteria were characterized using small-angle X-ray scattering (SAXS) and JEM-2100F TEM system (JEOL; Peabody, MA). The microscope was operated at 200 kV. Bright-field and selected area diffraction (SAD) digital images were collected using an 11 megapixel Orius SC1000 charge-coupled device camera (Gatan, Inc.; Pleasanton, CA). SAD patterns were collected from areas that included numerous magnetosomes using a nominal camera length of 25 cm, which had previously been calibrated against a polycrystalline gold sample. The scanning transmission electron microscopy (STEM) mode was used to collect STEM high-angle annular dark field (HAADF) images with a Gatan 806 HAADF detector. The collection angle range was 48–168 mrad.

2.6.2 Electron Energy-Loss and X-ray Energy Dispersive Spectra

Electron energy-loss spectroscopy (EELS) and X-ray energy dispersive spectroscopy (XEDS) spectra were obtained in STEM mode while using HAADF imaging. The HAADF4 camera length had an acquisition range of 45 to 145 mrad and a convergence angle of 8.3 mrad. A spot size of 0.2 nm was used for imaging and EELS modes, and the probe current was approximately 95 pA. The Gatan Microscopy Suite version 1.85 with the DigiScan system (Gatan) was used to collect all of the TEM and STEM images and the EELS spectra. EELS spectra were collected using a Tridiem imaging filter (Gatan) in spectrometer mode. The collection angle was 9.7 mrad, the dispersion was 0.3 eV per channel, and the energy resolution was 1.2 eV. Zero loss spectra were collected using an exposure of 0.01 s. Core loss spectra, which included the O–K and Fe–$L_{2,3}$ edges, were obtained in Cumulative mode. The exposure was 0.5 s for each frame until it was manually stopped, when the counts in the last channel of the spectrum were visually determined to be approximately 2×10^4. This was typically about 60–70 s (120–140 frames). The acquisition was performed while scanning on a single particle in Preview mode with a 512 × 512 pixel window, a 4 µs dwell time, and a 50,000,000× magnification. The XEDS system used was an Octane 30 Elite system (EDAX; Mahwah, NJ) with a windowless detector. Spectra were acquired using a 1 nm probe size with an approximately 780 pA probe current.

2.6.3 SAXS

SAXS was performed on magnetosome samples collected from *M. Gryphiswaldense*. The magnetosomes were provided as a stock dispersion of particles in water and were characterized as provided. The dispersion was placed in Kapton film (DuPont; Wilmington, DE) capillaries, which were then sealed with rapid-curing epoxy. SAXS data were collected on an S-MAX3000 SAXS instrument (Rigaku Americas Corporation; The Woodlands, TX) with Cu-Kα X-rays (wavelength [λ] of 1.542 Å) generated at 40 kW and focused using a collimating optic. Data were collected using a two-dimensional multiwire gas-filled detector at a sample-to-detector distance of 150 cm. The raw data from the sample were corrected for transmission and background noise prior to conversion to one dimension through azimuthal averaging. One-dimensional SAXS data are presented as intensity, $I(q)$, as a function of the magnitude of the reciprocal scattering vector, q, where $q = 4\pi \cdot \sin(\theta)/\lambda$, and where 2θ is the scattering angle. From Bragg's law, it follows that $q = 2\pi/d$, where d is distance. Following the

procedure described by Pedersen, the low-angle data were also corrected for shadowing by the beamstop.[15] Data processing and corrections were performed using Igor Pro, version 7.08 (Wavemetrics, Inc.; Portland, OR) software and procedures provided by Argonne National Laboratory (Lemont, IL).[16] Analysis of the form-factor scattering was performed in MATLAB R2018a (MathWorks; Natick, MA) using procedures provided by Argonne National Laboratory.[17,18]

3. RESULTS AND DISCUSSION

3.1 Growth of Flask Cultures

Flask cultures were monitored by measuring the OD_{600} to establish a growth curve. The curve (Figure 1) illustrates how slowly *M. Gryphiswaldense* grew. The alpha culture (in red) was started directly from a glycerol stock. Beta (in green) was started 24 h after alpha, from a 1:10 dilution of the alpha culture. The right-shift of the beta culture graph can be explained by the manner in which it was started: the cultures were not of the same starting density, which likely caused a prolonged lag phase in the beta culture. The general shape of each curve is the same, and each culture entered into log phase by 0.1 nm and approached stationary by 0.35 nm. It is apparent from the graph that *M. gryphiswaldense* grows very slowly. By comparison, an *Escherichia coli* growth curve can be completed in 12 h; this experiment went on for over 60 h. This data highlights why alternative methods such as fermentation (to do scale up and production) are necessary when working with *M. gryphiswaldense* .

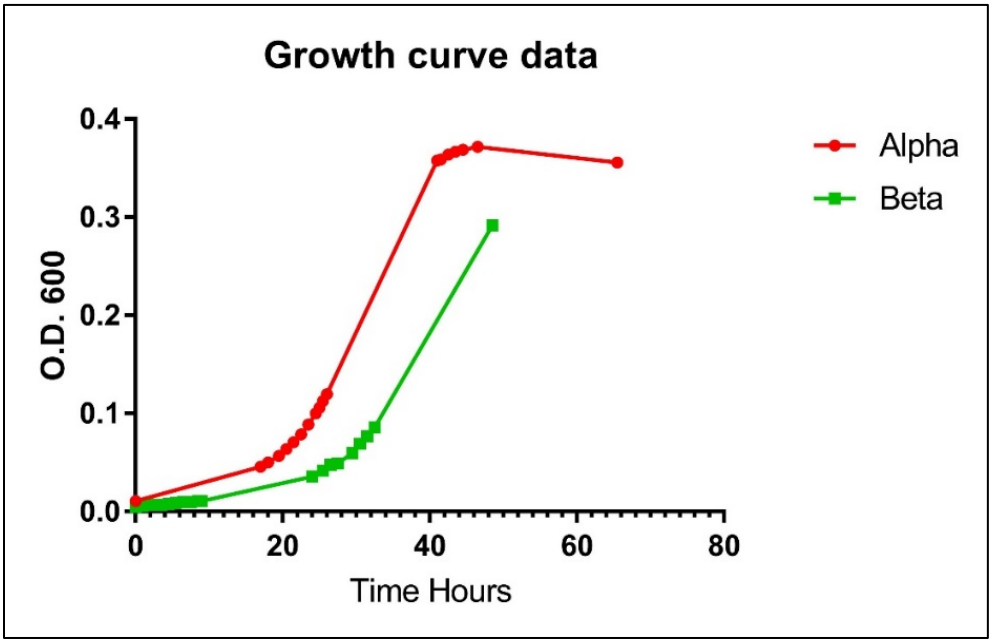

Figure 1. Growth curve of *M. gryphiswaldense* 100 mL flask cultures. This graph shows the growth of *M. gryphiswaldense* over several days in a 100 mL flask.

3.2 Formation and Verification of Magnetosomes in *M. gryphiswaldense*

Flask cultures of *M. gryphiswaldense* indicated that magnetosome formation inside the bacteria was occurring (Figure 2A). In addition to a color change from white to brown, the results of the "magnetic race track" and other magnetic methods used to verify the development of mNPs showed the response of the bacteria to the neodymium iron boron magnet (Figure 2B,C).

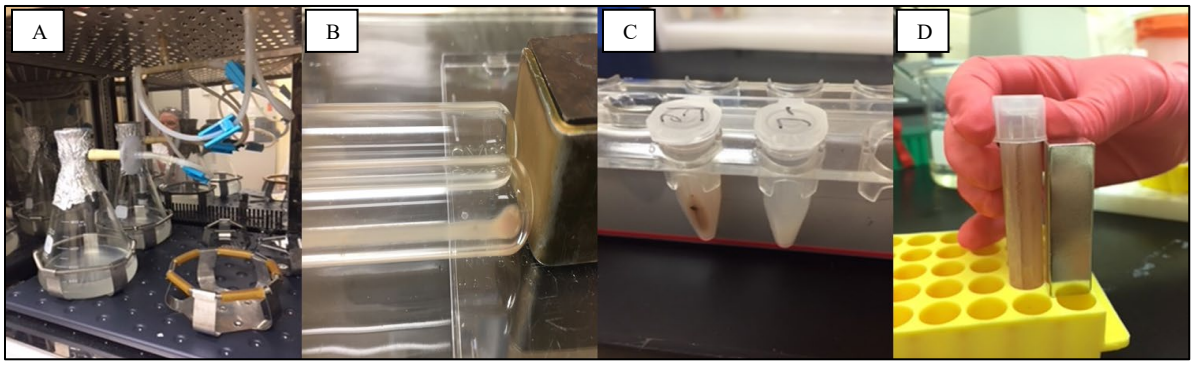

Figure 2. Verification of magnetosome formation. (A) Flask culture of *M. gryphiswaldense*. (B) Magnetic "race track" showing the movement of *M. gryphiswaldense* toward a magnet. (C and D) 1 mL and 5 mL tubes, respectively, showing magnetosome concentrations on the sides of the tubes after incubation with a magnet.

3.3 Magnetosome Yield

The yield of magnetosomes was calculated by weighing the bacteria before purification and then weighing the dehydrated magnetosomes after purification. The yield was expressed as milligrams of magnetosomes per gram of wet pellet (Table 1).

Table 1. Magnetosome Yield

Trial No.	Wet Cell Paste (g)	Magnetosomes (mg)	Yield (mg/g)
1	11.0	50.0	4.54
2	14.8	59.4	3.9
3	13.76	16.1	1.17

Note: Table 1 records the weights of starting and final material from magnetosome purification. Yield was calculated as milligrams of magnetosomes per gram of cell paste.

Trial 3 was a bit of an outlier and can be explained by the accidental aspiration of some of the magnetic material during washing. Upon reflection, it would have been more useful to record the yield in terms of culture volume rather than wet pellet weight. However, due to limitations in processing volumes, chunks of frozen cell paste were taken from a large block that was stored in the freezer. In the future, it would be better to have evenly distributed aliquots of paste to make the calculations more accurate.

3.4 TEM Analysis

TEM analysis indicated that the magnetosomes were, on average, 40 nm, and could be described as cubo-octohedral shaped (Figure 3A). TEM also showed that the dispersion and chain formation of the magnetosomes were dependent on the solution in which they were prepared. Experiments with drying and rehydrating indicated that although the magnetosomes retained their magnetism upon rehydration, they did not regain their ability to self-assemble into chains. The images also show areas of aggregation (Figure 3B,C).

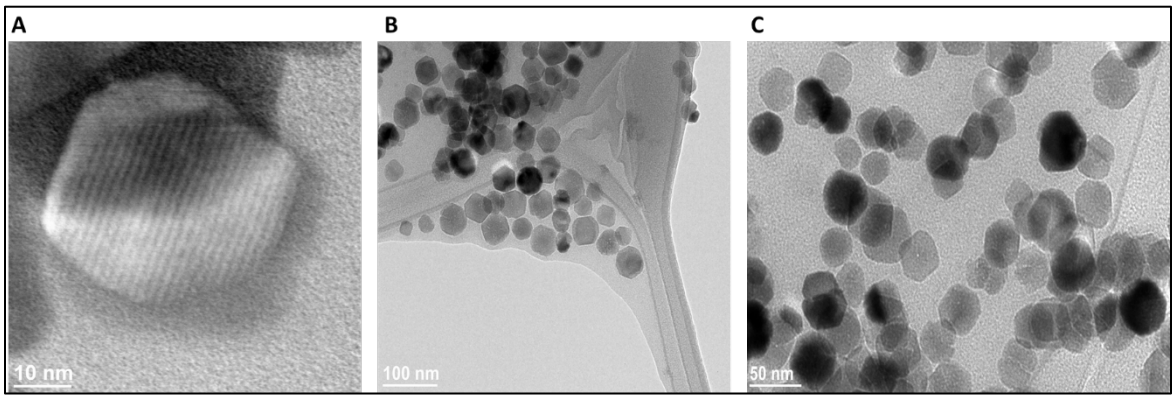

Figure 3. TEM analysis of mNPs. (A) Single mNP from *M. gryphiswaldense*. (B, C) Dried mNPs.

The experiments in storage with glycerol at –80 °C indicated that glycerol stocking is an acceptable but not optimal form of long-term storage for purified magnetosomes. Upon thawing and washing, the magnetosomes showed some propensity to aggregate. This may have been from residual glycerol. There is some evidence that magnetosomes are able to self-assemble into chains (Figure 4).

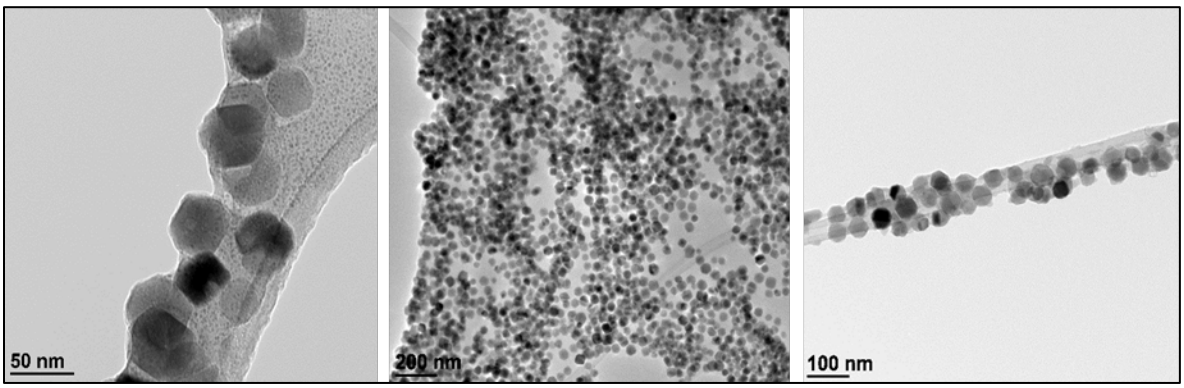

Figure 4. TEM images of purified magnetosomes at different magnifications. Magnetosomes were stored in 25% glycerol and frozen at –80 °C. Some aggregation was present, but they did retain the ability to self-assemble into chains.

Dehydration and storage in ethanol was deemed to be a better way to store magnetosomes. With use of this method, the magnetosomes were easily viewed via TEM, they maintained chain structure, and they were well dispersed (Figure 5).

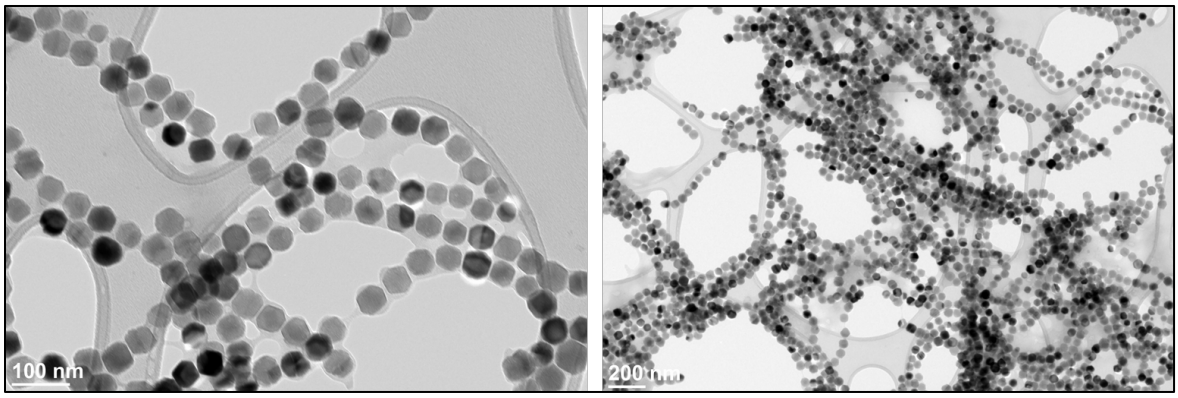

Figure 5. TEM images of magnetosomes that were dehydrated through an alcohol gradient and stored in 100% ethanol. Magnetosomes were well dispersed and readily formed chains.

Of all the storage conditions attempted, the worst was PBS, in which the magnetosomes aggregated (data not shown). The best diluent was 0.22 µm filtered tap water (Figure 6).

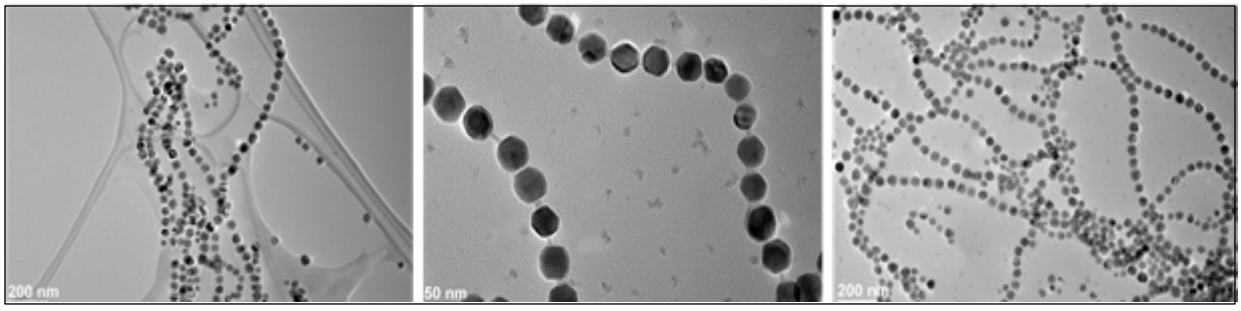

Figure 6. TEM images of magnetosomes from *M. gryphiswaldense* (at different magnifications) that were stored in 0.22 µm filtered tap water. Magnetosomes were clearly defined, well dispersed, and aligned in chains.

TEM was also used to view magnetosome formation inside whole bacteria. It was apparent that in any given preparation, only a fraction of the bacteria contained magnetosomes that were in chains of about 10 to 20 per organism (Figure 7).

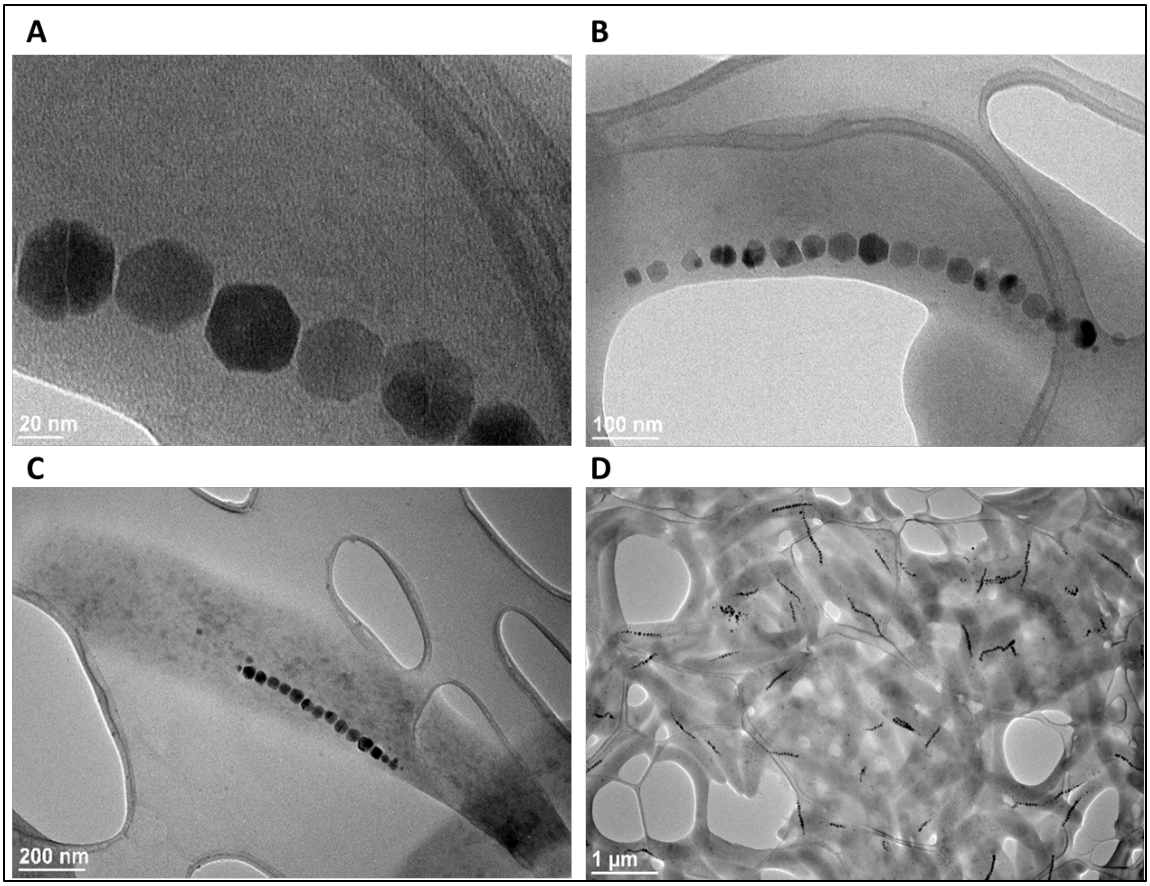

Figure 7. TEM images of *M. gryphiswaldense*. (A–C) *M. gryphiswaldense* with magnetosomes. (D) Lower magnification view of *M. gryphiswaldense*. Only a fraction of the bacteria contained magnetosomes.

3.5 SAD

A SAD pattern was collected from an area that included numerous magnetosomes (Figure 8). The SAD pattern acquired in the Gatan digital format was imported and analyzed using CSpot software, version 2.0 (CrystOrient Krzysztof Sztwiertnia; Zabierzów, Poland; http://crystorient.com/cspot-software). The software was used to compare simulated ring patterns that were calculated from known Crystallographic Information File (CIF) phases of iron oxides found in the Crystallography Open Database (International Union of Crystallography; Chester, England; http://www.crystallography.net/cod/). As shown in Figure 8, the diffraction pattern is very well matched for the magnetite phase given by CIF no. 1539747 and is identified as Fe_3O_4.

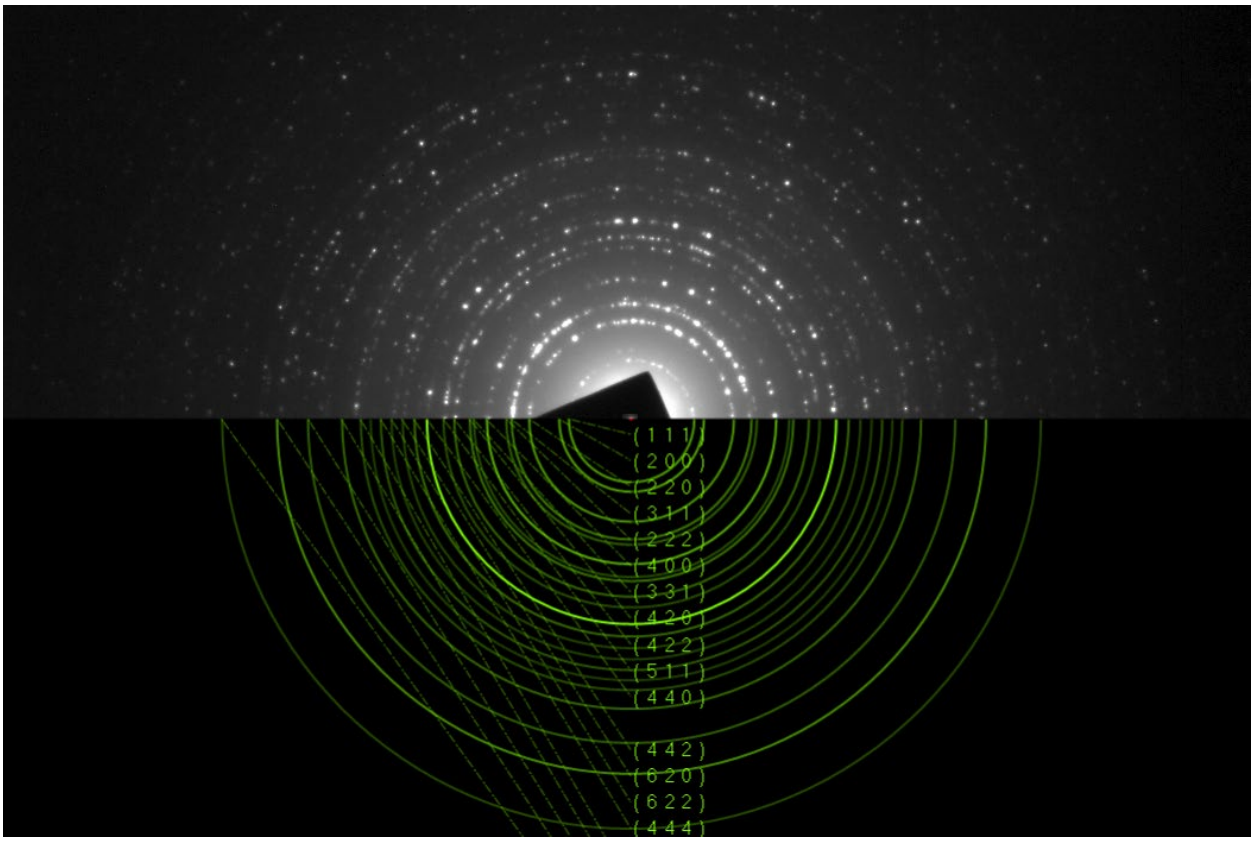

Figure 8. SAD pattern of magnetosomes with the magnetite Fe_3O_4 phase (CIF no. 1539747) overlaid and indexed.

3.6 EELS

The relative thickness measured from the low loss spectrum of a single magnetosome (shown in Figure 9A) was consistently about 0.23 for single particles. Figure 9B shows the low loss spectrum for a single particle after background-subtraction and correction for plural scattering. From the quantitative analysis of the EELS data (Figure 9), the atomic concentrations of Fe and O were 43.4 and 56.6, respectively, with about a 10% error. These give an Fe/O atomic ratio of 0.77, which agrees well with 0.75 for Fe_3O_4.

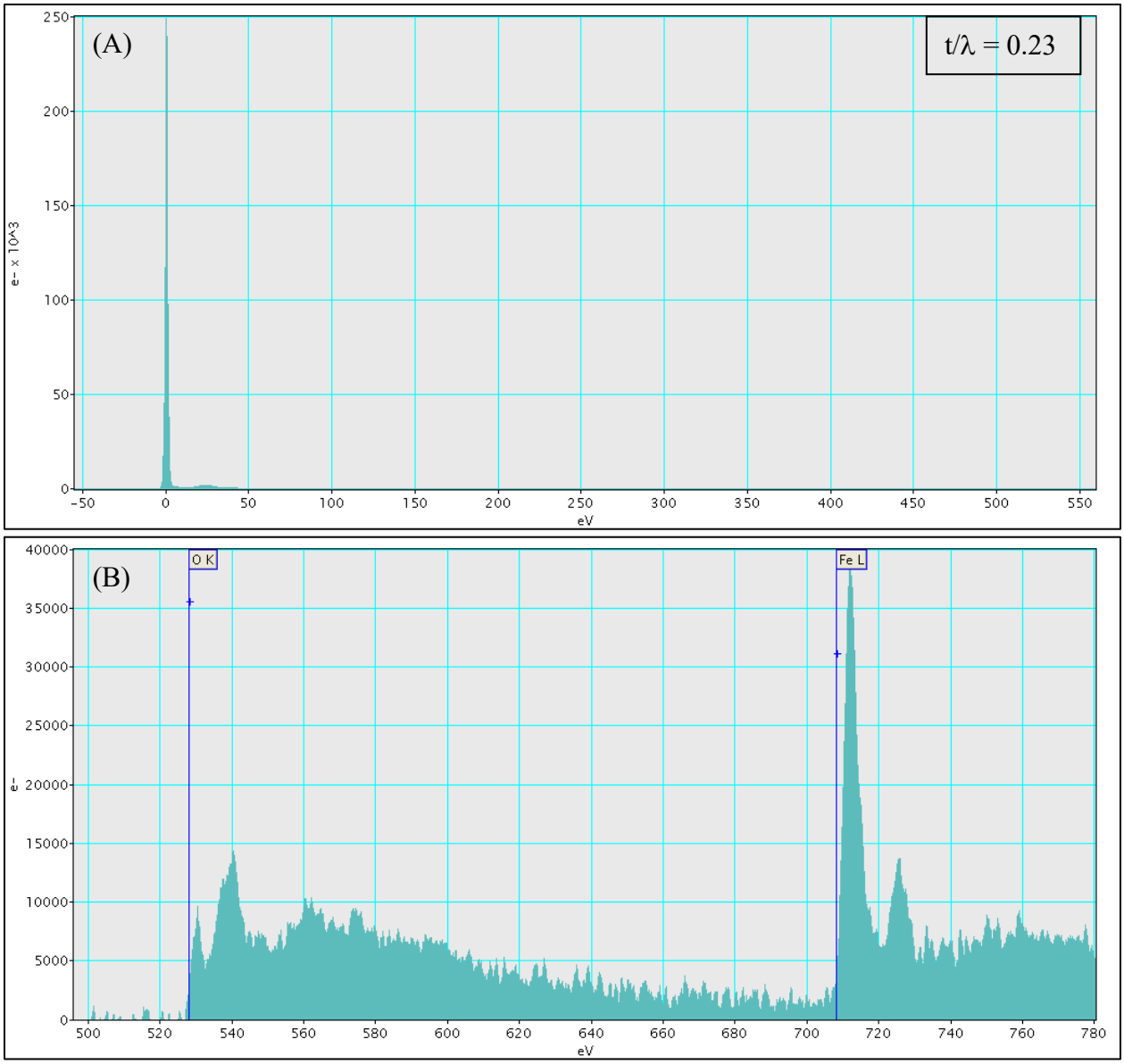

Figure 9. EELS data acquired from a single magnetosome. (A) Low loss spectrum. (B) Core loss spectrum, which includes the O–K and Fe–$L_{2,3}$ edges. The core loss spectrum was background-subtracted and corrected for plural scattering.

3.7 XEDS

Figure 10 shows an XEDS spectrum of a single magnetosome acquired in STEM mode using a 1 nm probe. The spectrum only identifies the presence of Fe and O from the particle. The analysis of O with XEDS is notoriously poor, and the XEDS spectrum was only used to identify the elements present and thereby ensure that no elements in EELS were missed using that method of analysis.

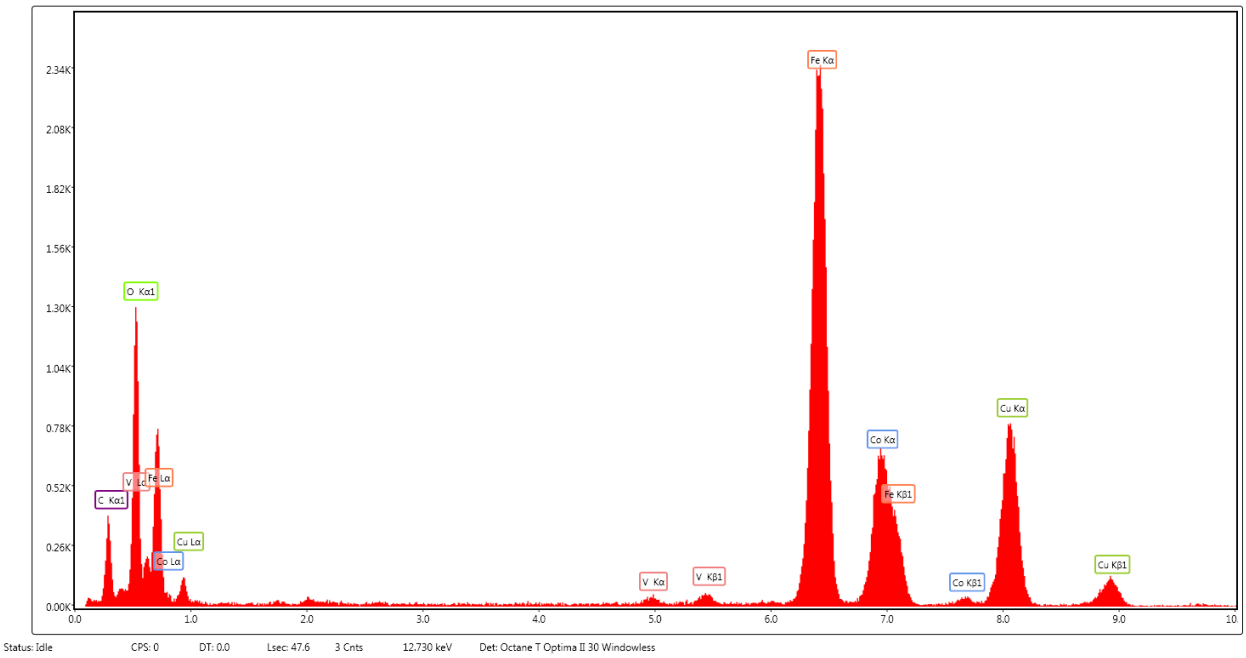

Figure 10. XEDS spectrum of a single magnetosome showing the Fe and O present. The small V and Co peaks are artefacts from the microscope. The Cu peaks are from the support grid, and the C peak is from the support film.

3.8 Characterization and Analysis of mNPs Using SAXS

Characterization of NPs using SAXS is a well-developed technique.[19] The scattering from NPs is influenced by particle shape, size dispersity, and concentration.[17] In the case of dilute particles, form-factor scattering is observed.[20] As the particles become more concentrated, interparticle scattering (structure) begins to affect the data, making particle shape and size identification difficult, if not impossible.[21] In the present study, magnetosomes generated by *M. gryphiswaldense* were known to be Fe_3O_4 NPs with a cubo-octohedral shape and an average particle diameter of 38–45 nm.[22–24] The cubo-octahedron is an Archimedean solid comprising six triangular faces and eight square faces. All edges are identical in length, and the edge length is equal to the distance from the center to each vertex.

The results of the SAXS analysis are shown in Figure 11. The data clearly show a typical Guinier "knee" as well as a higher-order feature above the knee, which is presumed to be a form-factor fringe. The absence of well-defined form-factor fringes above the knee indicates that there is some size dispersity in the particle dimension (e.g., diameter or edge length). The best fit of the form factor for a cubo-octohedron is also shown and was obtained for an edge length of 19.5 nm with a standard deviation of 3.5 nm. This would correspond to an average particle diameter of 39 nm, which is consistent with the previous reports.

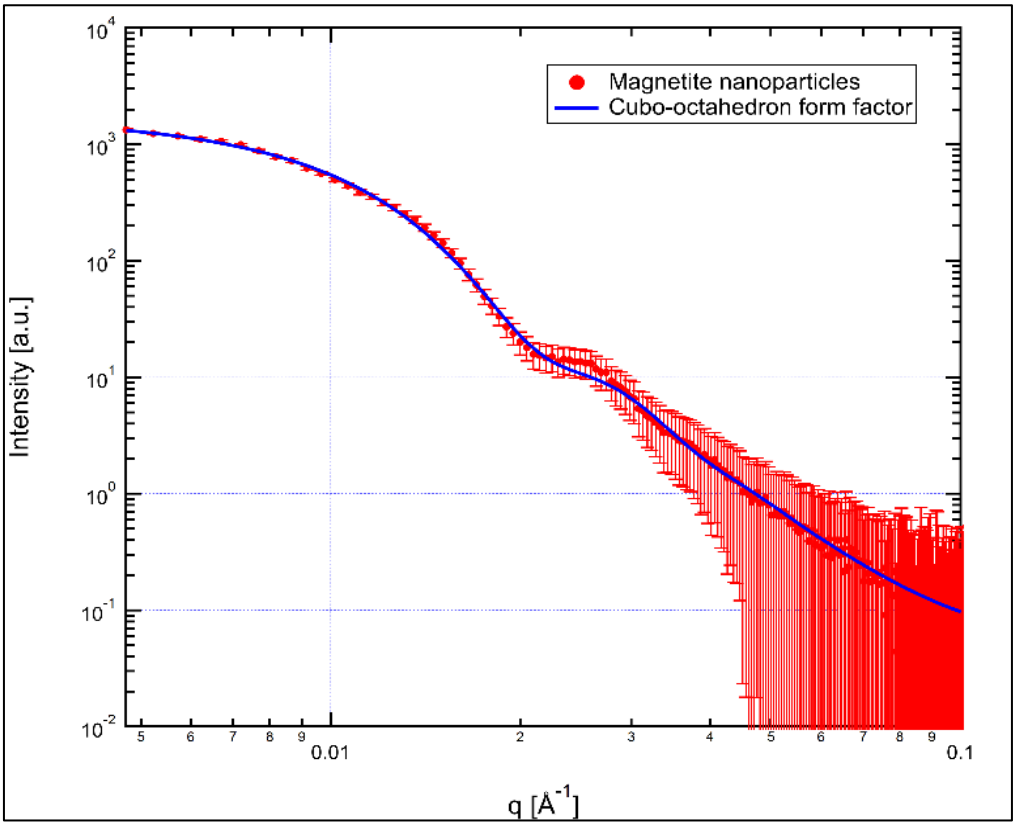

Figure 11. SAXS data for magnetosomes from *M. gryphiswaldense*. The best fit of the form factor is for cubo-octahedral particles having an edge length of 19.5 nm.

Although the cubo-octahedral form factor fits the data well through the Guinier knee and at higher angles, the fit breaks down at intermediate q (0.02–0.04 Å^{-1}), where the first fringe is present. There are at least two possible reasons for this discrepancy. First, it is possible that the shape was not cubo-octahedral. However, the TEM data presented in Figure 3 indicates that these magnetosomes were clearly faceted, and were at least consistent with a cubo-octahedral shape. Second, it is likely that some structure-factor effects are included in the SAXS data. Magnetosomes are well known for their magnetic character and ability to form chains of particles, such as the ones shown in Figure 6. Chaining of the mNPs would render them nondilute. Indeed, if one models the magnetosome chains as cylinders 40 nm in diameter and with length >> diameter, the form-factor scatter of such a cylinder corresponds well with the experimental data in the intermediate q region (see Figure 12). Nevertheless, the fit of a cylinder is unsatisfactory; large discrepancies dominate in the low q regime, where scattered intensity is high and error is low. The data are much more like those expected for 39 nm diameter cubo-octahedral mNPs than for long cylinders of the same diameter.

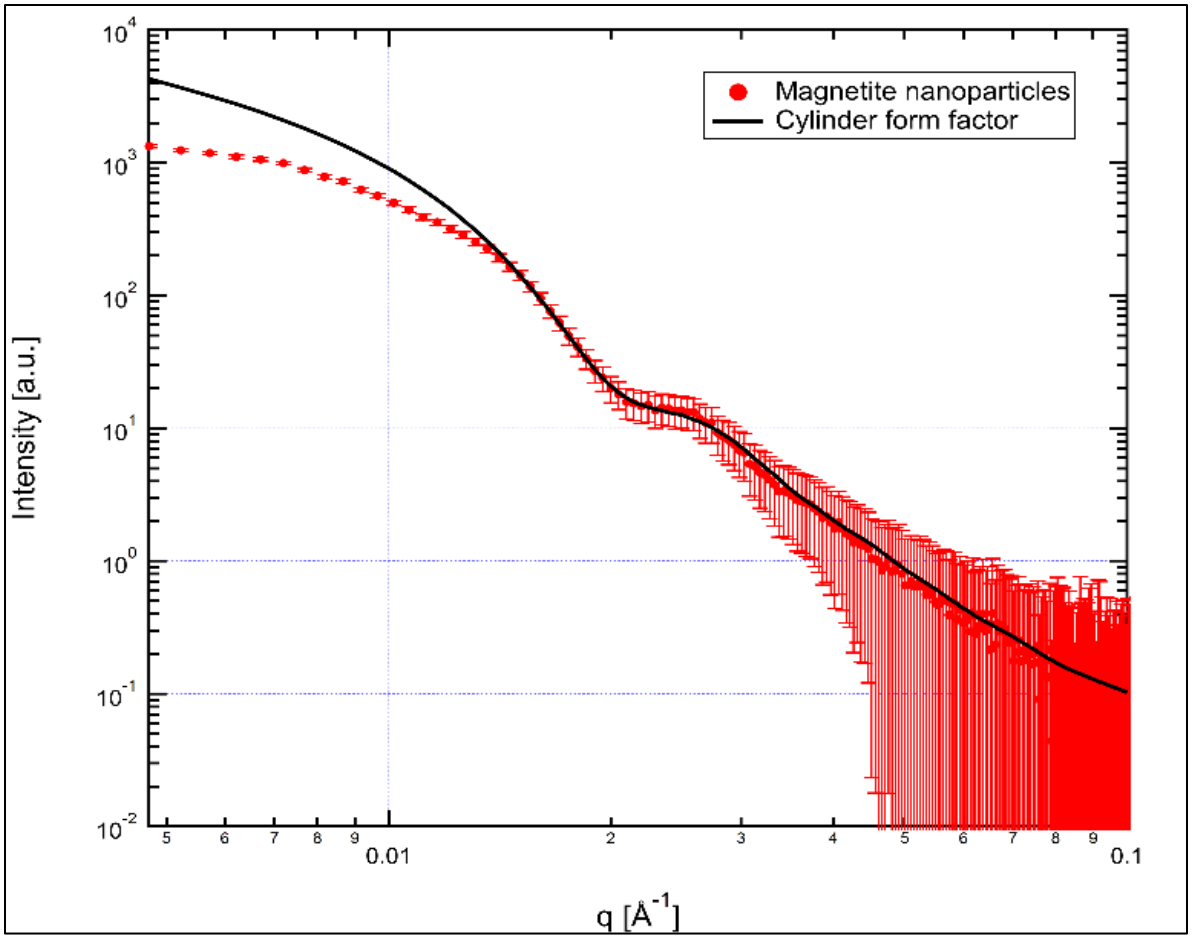

Figure 12. Example of form-factor scatter from cylindrical objects with the same diameter as the magnetosomes.

4. CONCLUSION

The freshwater bacteria *M. gryphiswaldense* was acquired from DSMZ and cultured in the laboratory. Both flask cultures and fermentation were used to grow *M. gryphiswaldense* and induce magnetosome formation. The magnetosomes were purified and characterized by a variety of spectroscopy techniques. This demonstrated that we have established physical criteria and storage methods for mNPs here at CCDC CBC. The magnetosomes produced by *M. gryphiswaldense* have a uniform size of approximately 40 nM and consist of a membrane-bound Fe_3O_4 nanocrystal that is cubo-octahedral in shape. Long-term storage can be achieved in 25% glycerol at –80 °C or in ethanol at 4 °C. *M. gryphiswaldense* is a slow-growing microaerophilic bacteria that only produces magnetosomes under conditions of oxygen deprivation. During the course of this study, we achieved yields between 1.1 and 4.5 mg of magnetosomes per gram of cell paste. In the future, we plan to record data as milligrams of magnetosomes per liter of culture as a more descriptive and useful measurement of yield. This work establishes a new capability of production of biologically derived mNPs at CCDC CBC. Additional work is necessary to improve yield, which is the current focus in academia and in private-industry laboratories to make this process more applicable to industrial use. We

recommend that CCDC CBC continue to invest in this promising field, given many applications are relevant to the mission in the fields of detection and shielding. Additional funding of approximately 100 work-hours is required to produce enough magnetosome material necessary to perform the shielding experiment that we have proposed as follow-on work. We have selected Keystone Compliance (Newcastle, PA), a company capable of testing to military specification standards in the frequency range of 10 kHz to 18 GHz, to perform the testing. The estimated additional cost will be $5800.

REFERENCES

1. NORAD Moving Comms Gear Back to Mountain Bunker. *Defense News,* 8 April 2018; https://www.defensenews.com/global/the-americas/2015/04/08/norad-moving-comms-gear-back-to-mountain-bunker (accessed 17 March 2020).
2. Army to Build Blast- and EMP-Proof Launch-Control Building for Alaska-Based Missile Defense. *Military and Aerospace Electronics,* 19 May 2014. http://www.militaryaerospace.com/articles/2014/05/emp-proof-building.html (accessed 17 March 2020).
3. Protecting Technological Infrastructure with EMP-Proof Conductive Concrete. *All About Circuits,* 4 December 2016; https://www.allaboutcircuits.com/news/protecting-technological-infrastructure-with-emp-proof-conductive-concrete/ (accessed 17 March 2020).
4. Moon, J.-W.; Rawn, C.J.; Rondinone, A.J.; Love, A.J.; Roh, Y.; Everett, S.M.; Lauf, R.J.; Phelps, T.J. Large-Scale Production of Magnetic Nanoparticles Using Bacterial Fermentation. *J. Ind. Microbiol. Biotechnol.* **2010,** *37* (10), 1023–1031.
5. Maher, B.A; Ahmed, I.A.M.; Karloukovski, V.; MacLaren, D.A.; Foulds, P.G.; Allsop, D.A.; Mann, D.M.A.; Torres-Jardón, R.; Calderon-Garciduenas, L. Magnetite Pollution Nanoparticles in the Human Brain. *PNAS: Proc. Natl. Acad. Sci. U.S.A.* **2016,** *113* (39), 10797–10801; http://www.pnas.org/content/113/39/10797.full.pdf (accessed 17 March 2020).
6. Vargas, G.; Cypriano, J.; Correa, T.; Leão, P.; Bazylinski, D.A.; Abreu, F. Applications of Magnetotactic Bacteria, Magnetosomes and Magnetosome Crystals in Biotechnology and Nanotechnology: Mini-Review. *Molecules* **2018,** *23* (10), 2438; https://www.mdpi.com/1420-3049/23/10/2438 (accessed 17 March 2020).
7. Fernández-Castané, A.; Li, H.; Thomas, O.R.T.; Overton, T.W. Development of a Simple Intensified Fermentation Strategy for Growth of *Magnetospirillum gryphiswaldense* MSR-1: Physiological Responses to Changing Environmental Conditions. *N Biotechnol* **2018,** *46,* 22–30.
8. Lefèvre, C.T.; Bazylinski, D.A. Ecology, Diversity and Evolution of Magnetotactic Bacteria. *Microbiol. Mol. Biol. Rev.* **2013,** *77* (3), 497–526.
9. Yan, L.; Zhang, S.; Chen, P.; Liu, H.; Yin, H.; Li, H. Magnetotactic Bacteria, Magnetosomes and Their Application. *Microbiol. Res.* **2012,** *167,* 507–519.
10. Xiang, L.; Wei, J.; Sun, J.; Guili, W.; Guan, F.; Ying, L. Purified and Sterilized Magnetosomes from *Magnetospirillum gryphiswaldense* MSR-1 Were Not Toxic to Mouse Fibroblasts in Vitro. *Lett. Appl. Microbiol.* **2007,** *45* (1), 75–81; https://doi.org/10.1111/j.1472-765X.2007.02143.x (accessed 17 March 2020).
11. Headquarters, Department of the Army. *The Army's Energy Security and Sustainability (ES2) Strategy*, 2015; https://www.army.mil/e2/c/downloads/394128.pdf (accessed 17 March 2020).

12. Hungate, R.E. A Roll Tube Method for Cultivation of Strict Anaerobes. *Methods Microbiol.* **1969,** *3* (B), 117–132.

13. Zhang, Y.; Zhang, X.; Jian, W.; Ying, L.; Li, J. Semicontinuous Culture of *Magnetospirillum gryphiswaldense* MSR-1 Cells in an Autofermenter by Nutrient-Balanced and Isosmotic Feeding Strategies. *Appl. Environ. Microbiol.* **2011,** *77* (17), 5851–5856.

14. DSMZ GmbH. Microorganisms. 380. Magnetospirillum Medium. https://www.dsmz.de/microorganisms/medium/pdf/DSMZ_Medium380.pdf (accessed 17 March 2020).

15. Pedersen, J.S. A Flux- and Background-Optimized Version of the NanoSTAR Small-Angle X-ray Scattering Camera for Solution Scattering. *J. Appl. Cryst.* **2004,** *37,* 369–380.

16. Ilavsky, J. *Nika*: Software for Two-Dimensional Data Reduction. *J. Appl. Cryst.* **2012,** *45* (2), 324–328.

17. Li, T.; Senesi, A.J.; Lee, B. Small Angle X-ray Scattering for Nanoparticle Research. *Chem. Rev.* **2016,** *116* (18), 11128–11180.

18. Jones, M.R.; Macfarlane, R.J.; Lee, B.; Zhang, J.; Young, K.L.; Senesi, A.J.; Mirkin, C.A. DNA-Nanoparticle Superlattices Formed from Anisotropic Building Blocks. *Nat. Mater.* **2010,** *9* (11), 913–917.

19. Glatter, O.; Kratky, O., Eds. *Small Angle X-ray Scattering.* Academic Press: New York, 1982.

20. Chen, G.; Yu, W.; Singh, D.; Cookson, D.; Routbort, J. Application of SAXS to the Study of Particle-Size-Dependent Thermal Conductivity in Silica Nanofluids. *J. Nanopart. Res.* **2008,** *10* (7), 1109–1114.

21. Schaefer, D.W.; Rieker, T.; Agamalian, M.; Lin, J.S.; Fischer, D.; Sukumaran, S.; Chen, C.; Beaucage, G.; Herd, C.; Ivie, J. Multilevel Structure of Reinforcing Silica and Carbon. *J. Appl. Cryst.* **2000,** *33,* 587–591.

22. Schüler, D.; Baeuerlein, E. Iron Transport and Magnetite Crystal Formation of the Magnetic Bacterium *Magnetospirillum gryphiswaldense*. *Journal de Physique IV Colloque* **1997,** *07* (C1), 647–650.

23. Orue, I.; Marcano, L.; Bender, P.; García-Prieto, A.; Valencia, S.; Mawass, M.A.; Gil-Cartón, D.; Alba Venero, D.; Honecker, D.; García-Arribas, A.; Fernández Barquín, L.; Muela, A.; Fdez-Gubieda, M.L. Configuration of the Magnetosome Chain: A Natural Magnetic Nanoarchitecture. *Nanoscale* **2018,** *10* (16), 7407–7419.

24. Naresh, M.; Gopinadhan, K.; Sekhar, S.; Juneja, P.; Sharma, M.; Mittal, A. NSOM/HRTEM Characterization of Biologically Derived Cubo–Octahedral Nanomagnets. *IEEE Trans. Magn.* **2009,** *45* (10), 4861–4864.

ACRONYMS AND ABBREVIATIONS

BSC	biological safety cabinet
CIF	Crystallographic Information File
EELS	electron energy loss spectroscopy
EMP	electromagnetic pulse
HAADF	high-angle annular dark field
I (q)	intensity
mNP	magnetite nanoparticle
NP	nanoparticle
OD	optical density
PBS	phosphate-buffered saline
q	reciprocal scattering vector
RPM	rotations per minute
SAD	selected area diffraction
SAXS	small-angle X-ray scattering
STEM	scanning transmission electron microscopy
TEM	transmission electron microscopy
XEDS	X-ray dispersive spectroscopy

DISTRIBUTION LIST

The following individuals and organizations were provided with one Adobe pdf electronic version of this report:

U.S. Army Combat Capabilities Development
Command Chemical Biological Center
(CCDC CBC)
FCDD-CBR-BM
ATTN: Calm, A.
Basi, K.

U.S. Army Combat Capabilities Development
Command Army Research Laboratory
ATTN: Walck, S.
Beyer, F.
Savage, A.

CCDC CBC Technical Library
FCDD-CBR-L
ATTN: Foppiano, S.
Stein, J.

Defense Technical Information Center
ATTN: DTIC OA

U.S. ARMY COMBAT CAPABILITIES DEVELOPMENT COMMAND
CHEMICAL BIOLOGICAL CENTER